Chapter 92
A Novel Immersed Framework of Computational Fluid Structure Interaction

Wang Xinyu, Chennakesava Kadapa, and Mei Yue

Abstract The interaction between fluid and immersed solid is a nonlinear multi-physical phenomenon in science and engineering. Due to the challenges of large structural deformation, topological changes in the fluid domain, complexity of the geometry of the structure and computational efficiency and robustness for simulating fluid structure interaction (FSI) problems, developing accurate and efficient finite element numerical methods has always been a research focus in the field of computational fluid dynamics. To overcome these difficulties, we present an efficient stabilised immersed framework involving finite element method called CutFEM and a second-order accurate staggered numerical scheme for fluid–solid coupling. In the following work, we apply this novel framework of computational FSI to several numerical examples to verify the efficiency and robustness of the proposed scheme, and the accuracy is also validated by the results by using the present scheme compared with the reference values.

Keywords Fluid structure interaction · CutFEM · Immersed boundary method · Staggered scheme

92.1 Introduction

Fluid structure interaction is frequently encountered in science and engineering. It specifically refers to the interaction between fluid and immersed solid, which is a nonlinear multi-physical phenomenon. The simulation of FSI is of great significance in science and engineering applications, such as blood flows in arteries and artificial heart valves in biomedicine, various valves, pumps, turbines and vibration of wind

W. Xinyu · M. Yue (✉)
Department of Engineering Mechanics, Dalian University of Technology, Dalian 116024, China
e-mail: meiyue@dlut.edu.cn

C. Kadapa
School of Engineering and the Built Environment, Edinburgh Napier University, Edinburgh EH10 5DT, UK

S. Li (ed.), *Computational and Experimental Simulations in Engineering*, Mechanisms and Machine Science 145, https://doi.org/10.1007/978-3-031-42987-3_92

turbine blades, response of bridges and high-rise buildings to wind and aeroelastic response of aircraft in engineering [1]. Due to the challenges of large structural deformation, topological changes in the fluid domain, complexity of the geometry of the structure and computational efficiency and robustness for simulating fluid structure interaction (FSI) problems, developing efficient and accurate finite element numerical methods has always been a focus and difficulty in the field of engineering. At present, the body-fitted mesh method based on arbitrary Lagrangian-Euler formula (ALE) is the most widely used in commercial software, which requires complex mesh shifting and re-meshing algorithms to capture large deformations of structures. The process of re-meshing includes a data-mapping strategy from old mesh to the new mesh which also introduces error [2]. Hence, low computational efficiency for generating body-fitted meshes and poor convergence for re-meshing algorithms limit the applicability of ALE formulation. To overcome these difficulties, we present an efficient stabilised immersed framework involving finite element method called Cut Finite Element Method (CutFEM) and a second-order accurate staggered numerical scheme for fluid–solid coupling. The key of our immersed framework is to solve the Navier–Stokes equation approximately by using the stabilised finite element method on the fixed background fluid mesh discretised with hierarchical B-splines, which does not need to re-mesh. The weak formulations employ the mixed Galerkin formulation with the streamline-upwind/Petrov Galerkin (SUPG)/pressure-stabilizing/Petrov Galerkin (PSPG) stabilization to obtain the numerical solutions of the incompressible Navier–Stokes equation [3]. At the same time, the weak-coupling staggered scheme is employed to solve the governing equations of fluid and structure in fluid–structure coupling [4]. The application of our computational framework is demonstrated very efficient and robust by simulation [5, 6].

The following work is organized as follows. In Sect. 92.2, we give a brief introduction of our stabilized immersed framework including CutFEM and the staggered scheme. In Sect. 92.3, we demonstrate the efficiency and robustness of the proposed scheme by using some numerical examples.

92.2 Theory

92.2.1 CutFEM Method

The fluid is assumed to be viscous, incompressible and laminar in our work. The governing equations of fluid are solved on Cartesian grids discretized by B-spline. The hierarchical B-spline curves can optimize the fluid grids near the immersed solids. Compared with traditional Lagrangian basis functions, B-spline functions have better performance due to their high-order continuity [7].

B-splines are piecewise continuous polynomial functions [8]. Figure 92.1 shows B-spline basis functions for different orders Q_1, Q_2 and Q_3, refer to linear, quadratic,

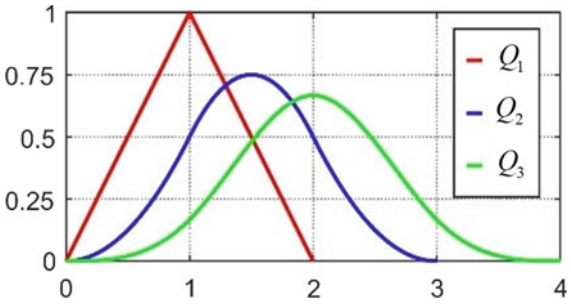

Fig. 92.1 One-dimensional univariate B-spline

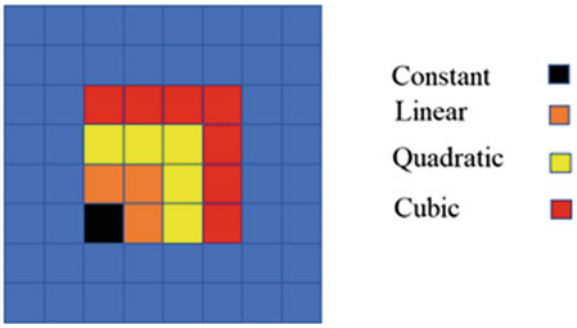

Fig. 92.2 B-Splines in 2D

cubic B-splines, respectively. For spatial discretization of the hierarchical B-spline grid is shown in Fig. 92.2.

For given the knot vector $p = \{\xi_0, \ldots, \xi_{n+b+1}\}$, is a non-decreasing set of coordinates, where b is the order of polynomials and n is the number of basis functions used for the construction of B-spline curves, defined in the interval $\left[\xi_i\ ,\ \xi_{i+b+1}\right]$. The B-spline basis functions $N_{i,b}$ are given as [5]

$$N_{i,0}(\xi) = \begin{cases} 1 \text{ if } \xi_i \leq \xi \leq \xi_{i+1} \\ 0 \text{ otherwise} \end{cases} \tag{92.1}$$

$$N_{i,b}(\xi) = \frac{\xi - \xi_i}{\xi_{i+b} - \xi_i} N_{i,b-1}(\xi) + \frac{\xi_{i+b+1} - \xi}{\xi_{i+b+1} - \xi_{i+1}} N_{i+1,b-1}(\xi) \tag{92.2}$$

The current main work presents a new computational framework motivated by the developments in body-unfitted methods proposed by Burman et al. [9]. CutFEM builds on a general finite element formulation for the approximation of PDEs. The basic idea behind CutFEM is to make the discretization as independent as possible of the geometric description and minimize the complexity of mesh generation [9]. Figure 92.3 shows that for a condition consisting of two domains: fluid domain Ω^f

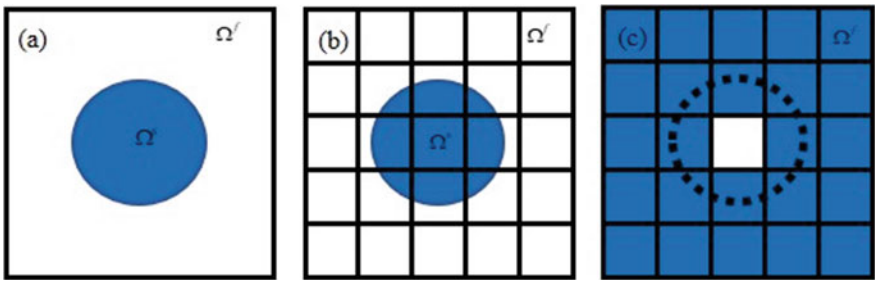

Fig. 92.3 Discretization: **a** geometry consisting of two domains **b** discretization with elements **c** elements belonging to the fluid domain Ω^f

and solid domain Ω^s and some cells of the background grid are cut by the interface between fluid domain and solid domain are cut-cells.

The accurate imposition of interface conditions is the key to the application of CutFEM. Boundary conditions can be imposed on the background grid by using Lagrange multiplier or penalty method [10]. However, the fluid mesh is not aligned with the boundary of the immersed solid, which increases the difficulty of imposing interface conditions. Number of researches have shown in recent studies [3] have proved that Nitsche method is an efficient and accurate strategy for boundary and interface conditions applied to the finite element formulation. Therefore, at the fluid–structure interface, we use Nitsche method to enhance the equilibrium of the fluid–structure interface [11]. Nitsche's method are applied in combination with the stabilization strategy to avoid the numerical instability associated with very small cutting elements [12]. The terms of Nitsche's method for enforcing the interface equilibrium conditions are as follows:

$$B_{\mathrm{N}}^{f}\left(\left\{\mathbf{w}^{f}, R\right\},\left\{\mathbf{v}^{f}, p\right\}\right)=\gamma_{\mathrm{N}_1}\int_{\Gamma_D}\mathbf{w}^{f}\cdot\left(\mathbf{v}^{f}-\mathbf{v}^{s}\right)d\Gamma-\int_{\Gamma_D}\mathbf{w}^{f}\cdot\left(\sigma\left(\left\{\mathbf{v}^{f}, p\right\}\right)\cdot\mathbf{n}^{f}\right)d\Gamma$$
$$-\gamma_{N}\int_{\Gamma_D}\left(\sigma\left(\left\{\mathbf{w}^{f}, R\right\}\right)\cdot\mathbf{n}^{f}\right)\cdot\left(\mathbf{v}^{f}-\mathbf{v}^{s}\right)d\Gamma \tag{92.3}$$

where n^f is the unit outward normal on the boundary Γ^f, σ is stress tensor. v^f and v^s is the velocity of the fluid and solid respectively. $\mathbf{w}^f$ and R are weight function of pressure and velocity, respectively. Γ is the boundary of the fluid. γ_{N_1} is a penalty parameter and $\gamma_{\mathrm{N}_1} \geq 0$. γ_{N_2} allows to choose between the symmetric $\gamma_{\mathrm{N}_2} = 1$ and the unsymmetric $\gamma_{\mathrm{N}_2} = -1$ variants of Nitsche's method [5].

If the intersections of boundary and cut element are very small, the system matrix may be very ill conditioned. The present work follows CutFEM, which uses ghost-penalty terms to alleviate numerical instability and to weakly enforce an appropriate amount of smoothness of the solution across the edges between the cut cells and across the edges between the cut cells and the interior cells (see Fig. 92.4), the ghost

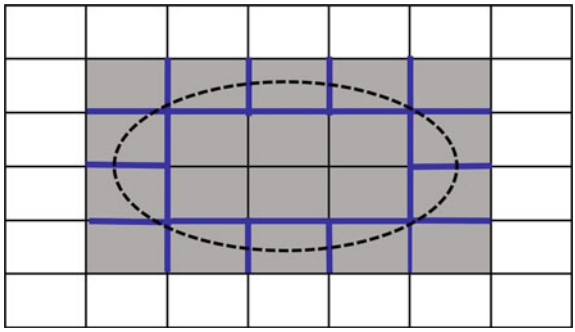

Fig. 92.4 Ghost-penalty operator is applied to the blue boundary

penalty term is defined as

$$\mathcal{B}^f_{\mathrm{GP}}(\{\mathbf{w}^f, R)\}, \{(\mathbf{v}^f, p)\}) = \gamma^u_{\mathrm{GP}}\mu\mathcal{G}_1\left(\mathbf{w}^f, \mathbf{v}^f\right) + \gamma^p_{\mathrm{GP}}\frac{1}{\mu}g_3(R, p) \tag{92.4}$$

where $\mathcal{B}^f_{\mathrm{GP}}(\{\mathbf{w}^f, R)\}, \{(\mathbf{v}, p)\})$ is the ghost-penalty term corresponding to the stability of the cut cells. $\mathcal{G}_1\left(\mathbf{w}^f, \mathbf{v}^f\right)$ is defined as jump operator as a vector-valued problem. γ^u_{GP} and γ^p_{GP} are the dimensionless ghost penalty parameters for velocity and pressure [5].

92.2.2 Staggered Scheme for Fluid Solid Coupling

The solution approach of fluid–structure coupling has a significant impact on the accuracy and efficiency of FSI numerical method. In FSI problems, the solution strategies are divided into strongly coupled and weakly coupled solution strategies. Based on Dirichlet–Neumann coupling, Dettmer et al. [6] proposed the second order accurate weakly coupled numerical scheme used for our present work.

The steps for the staggered scheme are described as follows. First, update time step $t_{n+1} = t_n + \Delta t$, and then predict force on the solid $F^{s^p}_{n+1}$, solve the solid problem for d^s_{n+1} and v^s_{n+1} using $F^{s^p}_{n+1}$. Then, reposition immersed solid, update cut cell data to get traction force F^f_{n+1} on fluid interface. After that, we introduce the relaxation factor β, The parameter β $(0 < \beta \leq 1)$ is defined as the relaxation factor. The value of β influence the stability of the proposed staggered solution strategy. Then use the formula $F_{n+1} = -\beta F^f_{n+1} + (1-\beta)F^{s^p}_{n+1}$ to correct the traction force on the solid. Finally, proceed to next time step. As demonstrated with the numerical examples [4, 6, 13], the application of this staggered scheme makes the FSI simulation very efficient.

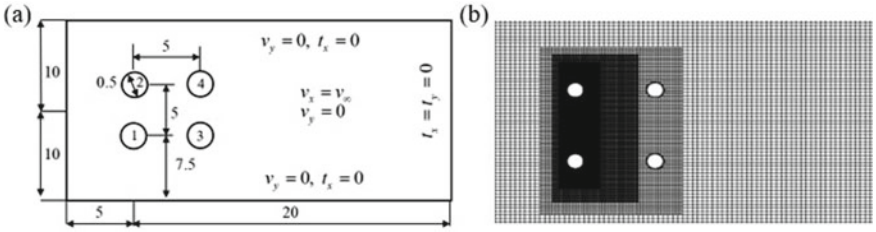

Fig. 92.5 Unsteady flow over cylinder bodies: **a** geometry and boundary condition **b** hierarchical b-spline mesh

92.3 Numerical Examples

92.3.1 Unsteady Flow Over Fixed Circular Bodies for Re = 100

The flow over the circular cylinders has always been focus in ocean engineering. The numerical simulations of two-dimensional flow around circular cylinders have been widely used in the field of ocean engineering. Due to the common phenomenon of interference between multiple cylinders, the research on the flow around multiple cylinders is of great significance.

In this numerical example, we employ our stabilized immersed framework to simulate. Figure 92.5 shows the geometry and boundary conditions of the problem and a level-3 hierarchical meshes discretized with B splines for simulations. Properties of the fluid are: density, $\rho^f = 10^3 \text{kg/m}^3$ and viscosity, $\mu^f = 1\,\text{kg/m s}$. The uniform velocity of $v_\infty = 1.0$ m/s is imposed at the inlet in X-direction so that the Reynolds number is $\text{Re} = \rho D v_\infty / \mu = 100$. Figure 92.6 shows flow over multiple fixed circular cylinders for $\text{Re} = 100$ of evolution of lift coefficient and drag coefficient, respectively. Due to the interference effect between the two cylinders, the drag coefficients of the upstream and downstream cylinders are different. Figure 92.6a shows the drag coefficients of the upper and lower cylinders with the same vertical y-axis almost overlap. For the upper and lower cylinders located on the same vertical y-axis, the lift curves shown in Fig. 92.6b are symmetric and illustrate that the near wake of two parallel cylinders is symmetrical and opposite. Figures 92.7b and 92.8b depict the symmetrical vortex shedding at the end of cylinders.

92.3.2 Vortex Induced Vibration of a Circular Cylinder

Vortex-induced vibration is one of the main causes of fatigue failure of structures. Therefore, the research on forced vibration and vortex-induced vibration of a cylinder

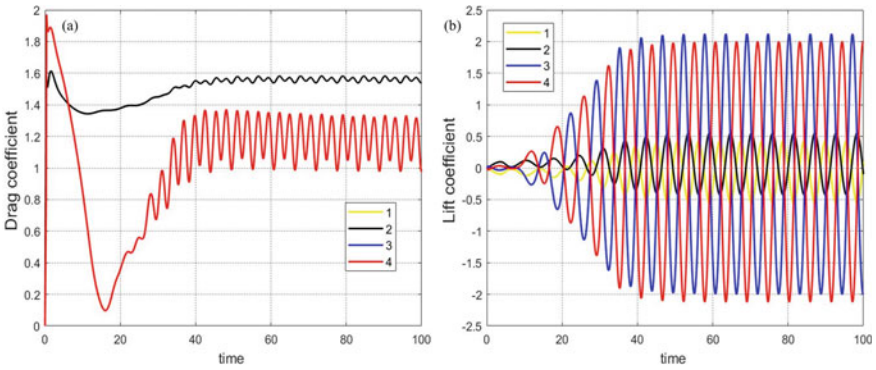

Fig. 92.6 Time history for flow over fixed cylinders of **a** drag coefficient **b** lift coefficient

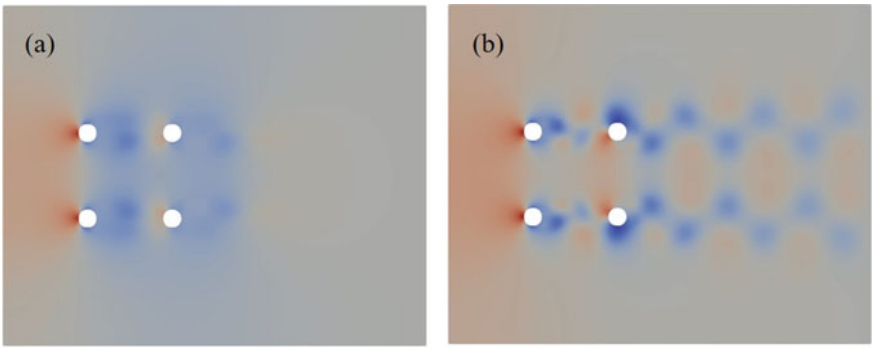

Fig. 92.7 Contours of pressure different time **a** $t = 10$ **b** $t = 100$

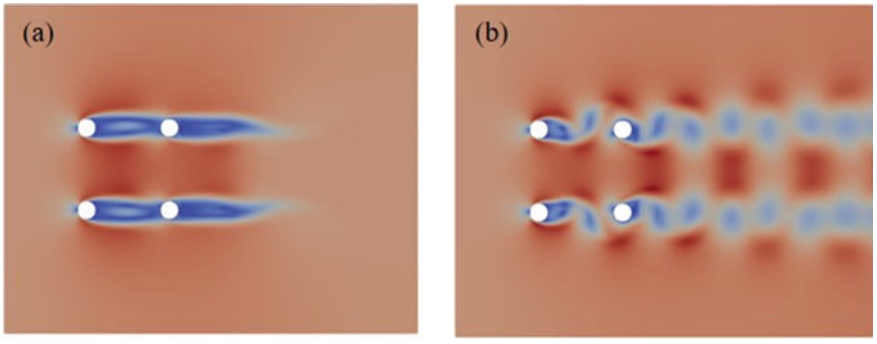

Fig. 92.8 Contours of velocity for different time **a** $t = 10$ **b** $t = 100$

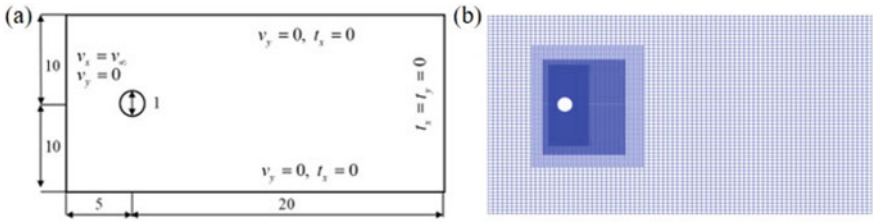

Fig. 92.9 VIV of circular cylinder: **a** geometry and boundary condition **b** hierarchical b-spline mesh

Table 92.1 The vibration response characteristics of cylinder system

Re	Vortex shedding frequency f_s	Normalized displacement
90	0.1440430	0.0012901
100	0.1654053	0.0029205
110	0.1986694	0.3505286
120	0.1989746	0.3394329
130	0.2282715	0.0060493

is of great significance for offshore engineering risers. The numerical example for VIV is concerned with an elastically mounted rigid circular cylinder.

The geometry and boundary conditions of this problem and hierarchical meshes discretized with B splines for simulations are shown as Fig. 92.9. The density of the fluid is $\rho^f = 10^3\,\mathrm{kg/m^3}$ and its viscosity is $\mu^f = 0.1\,\mathrm{kg/m\,s}$. For this example, we only consider the transverse degree of freedom. The properties of the structure are: mass, $m = 117.10\,\mathrm{g}$, the damping coefficient and stiffness are $c = 0.35317\,\mathrm{g/s}$ and $\mathrm{k} = 184.92\,\mathrm{g/s^2}$, respectively. The natural frequency $f_\mathrm{n} = 0.2\,\mathrm{Hz}$. We conduct simulations for Re within 90–130. The normalized values of the cylinder's displacement amplitude and vortex shedding frequency are shown in Table 92.1. It is observed from Fig. 92.10 that there is an interval where the vortex shedding frequency f_s coincides with the natural frequency $f_\mathrm{n} = 0.2\,\mathrm{Hz}$. The amplitude performed by the cylinder-spring system has the order of magnitude of the diameter of the cylinder in this Re interval. Figure 92.10 illustrates the amplitude values and the range of Re where the 'lock-in' occurs match well with other simulation results from the literature [14–17]. The results above-mentioned illustrate the capability of the immersed FSI framework.

92.3.3 Flexible Beam in Cross Flow

In this numerical example, we focus on the coupling of fluid and a flexible structure. The geometry and boundary conditions of this problem and hierarchical meshes

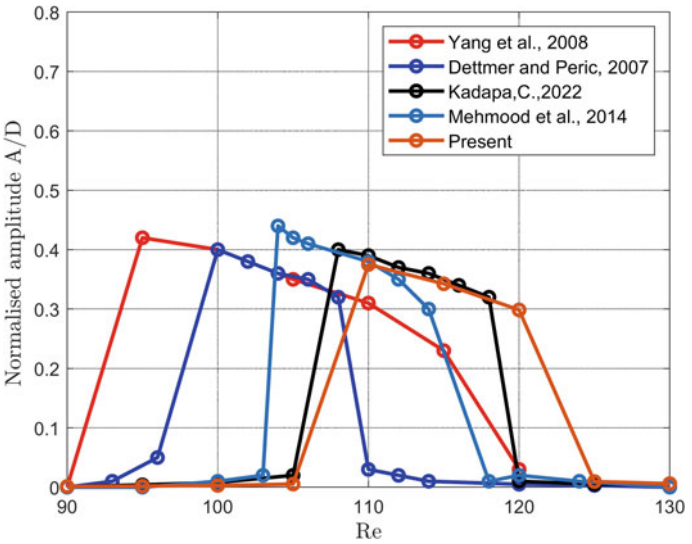

Fig. 92.10 Displacement amplitude of circular cylinder of vortex induced vibration

discretized with B splines for simulations are shown in Fig. 92.11. Properties of fluids: density, $\rho^f = 10^3\,\text{kg/m}^3$, and viscosity, $\mu^f = 0.1\,\text{kg/m s}$. Properties of structure: density, $\rho^s = 10^3\text{kg/m}^3$, Young's modulus, $E = 200\,\text{kPa}$ and Poisson's ratio $\nu^s = 0.3$. The inlet velocity is parabolic defined as $v_{in} = 20/6[y(0.6-y)]$. The time history of lateral displacement of point A and point B is shown in Fig. 92.12. The contour plots of fluid velocity at different times are shown in Fig. 92.13.

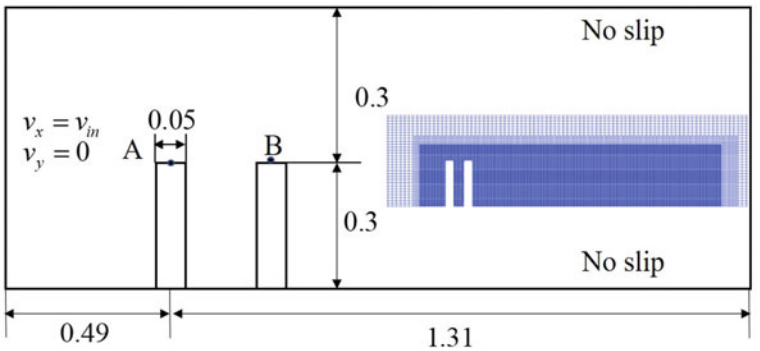

Fig. 92.11 Beam in cross flow: geometry, boundary condition and hierarchical B-spline mesh

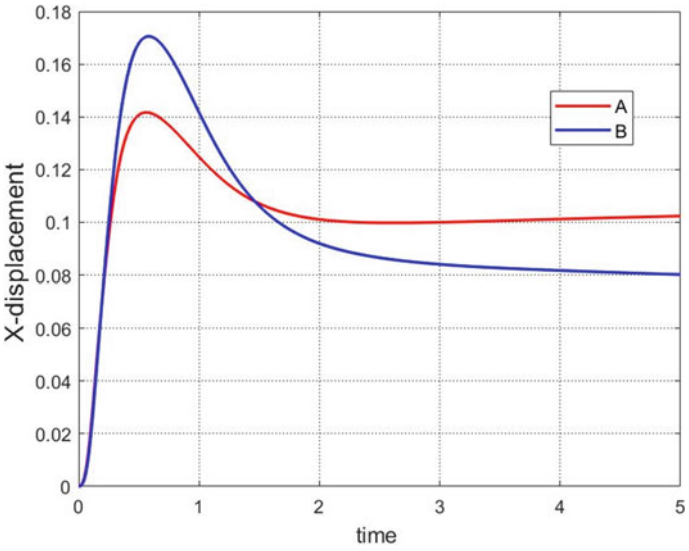

Fig. 92.12 Time history of X-displacement of point A and B

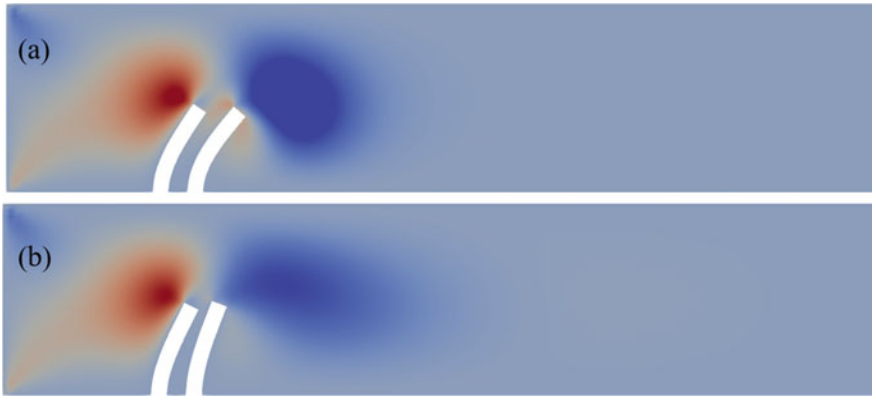

Fig. 92.13 Contour plots of fluid velocity at different times **a** $t = 1$ **b** $t = 5$

92.3.4 Vortex-Induced Vibrations of a Flexible Beam

We take this example as a benchmark example to test the fluid-flexible structure interaction. Figure 92.14 shows hierarchical meshes discretized with B splines and the geometry and boundary conditions of this problem. The density and viscosity of fluid are $\rho^f = 10^3 \text{kg/m}^3$ and $\mu^f = 1 \text{ kg/m s}$. The properties of this flexible structure are: density is $\rho^s = 10^4 \text{kg/m}^3$, Young's modulus is $E = 1.4 \times 10^6$ Pa and Poisson's ratio is $\nu^s = 0.4$.

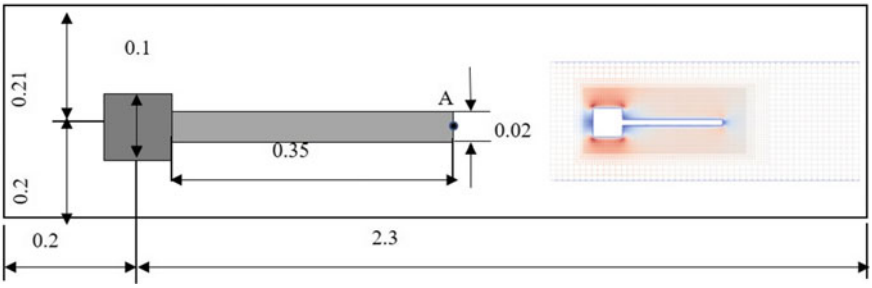

Fig. 92.14 Flexible beam: geometry, boundary condition and hierarchical B-spline mesh

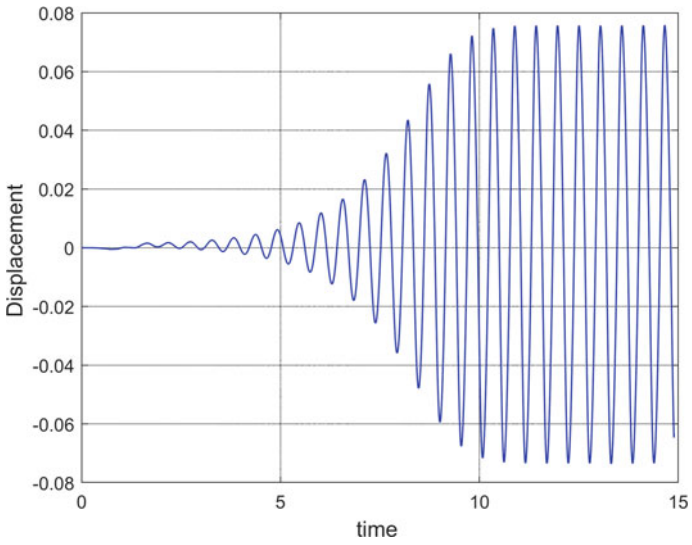

Fig. 92.15 Time history of Y-displacement of point A

The inlet velocity is defined as $v_{in} = 6/0.1681y(0.41 - y)$. The beam attached behind a fixed square body starts to oscillate due to vortices shedding by the corners of the square body.

Evolution of Y-displacement of the beam against time is presented in Fig. 92.15 and it shows the oscillation. Figure 92.16 shows the contour plots of velocity in x direction at two different times for the background meshes discretized with B splines.

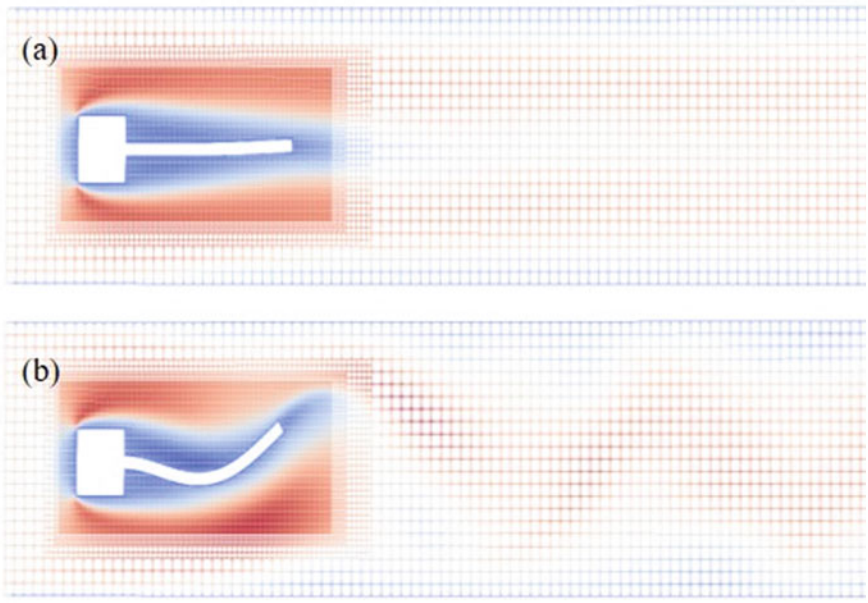

Fig. 92.16 Contour plots of fluid velocity at different times **a** $t = 5$ **b** $t = 12$

92.4 Conclusion

In our paper, we present an immersed stabilised framework for the simulation of fluid–structure interaction problems. We apply this numerical framework to several numerical examples and the robustness of the proposed scheme are demonstrated by the example of vortex induced vibration of flexible beam where the structure undergoes the large deformation, the example of flow over fixed cylinder demonstrated the efficiency of our proposed numerical scheme. As demonstrated with the example of VIV of cylinder, the accuracy is verified by the results obtained with our stabilized scheme are consistent with the reference value. The following research work is expected to employ this proposed framework to high performance computing architecture and large-scale industrial simulation.

References

1. Bazilevs, Y., Takizawa, K., Tezduyar, T.E.: Computational Fluid–Structure Interaction: Methods and Applications. Wiley, United Kingdom (2013)
2. Sahin, M., Mohseni, K.: An arbitrary Lagrangian-Eulerian formulation for the numerical simulation of flow patterns generated by the hydromedusa *Aequorea victoria*. J. Comput. Phys. **228**(12), 4588–4605 (2009)

3. Tezduyar, T.E., Mittal, S., Ray, S., et al.: Incompressible flow computations with stabilized bilinear and linear equal-order-interpolation velocity-pressure elements. Comput. Methods Appl. Mech. Eng. **95**(2), 221–242 (1992)
4. Kadapa, C., Dettmer, W.G., Perić, D.: Accurate iteration-free mixed-stabilised formulation for laminar incompressible Navier–Stokes: applications to fluid–structure interaction. J. Fluids Struct. **97**, 103077 (2020)
5. Kadapa, C., Dettmer, W., Perić, D.: A stabilised immersed framework on hierarchical b-spline grids for fluid-flexible structure interaction with solid–solid contact. Comput. Methods Appl. Mech. Eng. **335**, 472–489 (2015)
6. Dettmer, W.G., Lovrić, A., Kadapa, C., et al.: New iterative and staggered solution schemes for incompressible fluid-structure interaction based on Dirichlet-Neumann coupling. Int. J. Numer. Methods Eng. **122**(19), 5204–5235 (2021)
7. Schillinger, D., Rank, E.: An unfitted hp-adaptive finite element method based on hierarchical b-splines for interface problems of complex geometry. Comput. Methods Appl. Mech. Eng. **200**(47), 3358–3380 (2011)
8. Rüberg, T., Cirak, F.: A fixed-grid b-spline finite element technique for fluid–structure interaction. Int. J. Numer. Methods Fluids **74**(9), 623–660 (2014)
9. Burman, E., Claus, S., Hansbo, P., et al.: Cutfem: discretizing geometry and partial differential equations. Int. J. Numer. Methods Eng. **104**(7), 472–501 (2015)
10. Peskin, C.S.: The immersed boundary method. Acta Numer. **11**, 479–517 (2002)
11. Hansbo, P., Hermansson, J., Svedberg, T.: Nitsche's method combined with space–time finite elements for ale fluid–structure interaction problems. Comput. Methods Appl. Mech. Eng. **193**(39–41), 4195–4206 (2004)
12. Dettmer, W., Kadapa, C., Perić, D.: A stabilised immersed boundary method on hierarchical b-spline grids. Comput. Methods Appl. Mech. Eng. **311**, 415–437 (2016)
13. Kadapa, C.: A second-order accurate non-intrusive staggered scheme for the interaction of ultra-lightweight rigid bodies with fluid flow. Ocean Eng. **217**, 107940 (2020)
14. Yang, J., Preidikman, S., Balaras, E.: A strongly coupled, embedded-boundary method for fluid–structure interactions of elastically mounted rigid bodies. J. Fluids Struct. **24**(2), 167–182 (2008)
15. Dettmer, W.G., Perić, D.: A fully implicit computational strategy for strongly coupled fluid–solid interaction. Arch. Comput. Methods Eng. **14**(3), 205–247 (2007)
16. Kadapa, C.: A unified simulation framework for fluid–structure–control interaction problems with rigid and flexible structures. Int. J. Comput. Method **19**(01), 2150052 (2022)
17. Mehmood, A., Nayfeh, A.H., Hajj, M.R.: Effects of a non-linear energy sink (NES) on vortex-induced vibrations of a circular cylinder. Nonlinear Dyn. **77**, 667–680 (2014)